STARS

University of Central Florida
STARS

HIM 1990-2015

2014

Scalable Nano Particle Production of Low Bioavailability Pharmaceuticals for Augmented Aqueous Solubility

Aaron Madden
University of Central Florida

 Part of the Mechanical Engineering Commons
Find similar works at: https://stars.library.ucf.edu/honorstheses1990-2015
University of Central Florida Libraries http://library.ucf.edu

This Open Access is brought to you for free and open access by STARS. It has been accepted for inclusion in HIM 1990-2015 by an authorized administrator of STARS. For more information, please contact STARS@ucf.edu.

Recommended Citation

Madden, Aaron, "Scalable Nano Particle Production of Low Bioavailability Pharmaceuticals for Augmented Aqueous Solubility" (2014). *HIM 1990-2015*. 1800.
https://stars.library.ucf.edu/honorstheses1990-2015/1800

SCALABLE NANO PARTICLE PRODUCTION OF LOW BIOAVAILABILITY PHARMACEUTICALS FOR AUGMENTED AQUEOUS SOLUBILITY

by

AARON L. MADDEN

A thesis submitted in partial fulfillment of the requirements
for the Honors in the Major Program in Mechanical Engineering
in the College of Engineering and Computer Science
and in The Burnett Honors College
at the University of Central Florida
Orlando, Florida

Spring Term 2014

Thesis Chair: Dr. Wei Wei Deng

ABSTRACT

The billion dollar pharmaceutical research and development pipeline suffers greatly from high attrition rates of novel therapeutic compounds within pre-clinical and clinical trials. Poor bioavailability in many new drugs, originating in the various methodologies of high throughput screening, may explain part of these growing failure rates. One interpretation of this phenomenon relies on bioavailability's correlation with aqueous solubility; much modern processing allows chemicals to fully develop without touching water, yielding upwards of 90% of new chemical entities practically insoluble in aqueous media. Thus, one approach to alleviating bioavailability and potentially clinical attrition rates necessitates augmented aqueous solubility. The amorphous nanoparticle presents the largest boost in aqueous solubility of a chemical through processing alone.

In this contribution, we propose electrospray as a novel, competitive candidate to produce pharmaceutical amorphous nanoparticles with the intent of augmenting solubility. Electrospray represents an idyllic nominee for three reasons: repeatability, flexibility, and scalability. Electrospray offers low batch to batch variation with less than 30% relative standard deviation between various droplets. This triumphs over the several orders of magnitude in variation in pneumatic sprays. Electrospray's flexibility draws from its ability to attain diameters over several orders of magnitude, ranging from

hundreds of microns to several nanometers; in this contribution droplets are produced between 500 nm and 1 μm. Finally, electrospray displays scalability to any industrial requirement; though a single nozzle operates at mere microliters per hour, a single multiplexed array of emitters may increase this throughput by several orders of magnitude.

This exploration, utilizing Indomethacin as a model low solubility chemical, verifies electrospray as a compatible processing tool for the pharmaceutical industry. Scanning electron microscopy coupled with the image analysis software ImageJ gleans the size and shape of emitted (and dried) particles. Amorphicity verification of particles employs grazing angle x-ray diffraction. Finally, ultraviolet and visual spectrum spectroscopy evaluates the solubility advantage of particles.

DEDICATION

For my family,
You stand by me now
You've been shelter during rain
This work is for you

ACKNOWLEDGEMENTS

I owe a huge debt of gratitude to all the people who helped make this thesis possible. Most especially to Dr. Wei Wei Deng who provided infinite guidance and preparation in the field. To all the members of the Droplet and Energy Research lab who taught the technical tools of analysis and helped along the way. A great thanks to my committee members Dr. Hyoung Jin Cho and Dr. Andre Gesquiere for taking time from themselves to serve this effort. For each professor propelling me to new knowledge. To Kelly Astro and Denise Crisafi, no thesis could be written without your dedication. Finally to my family and all my friends.

TABLE OF CONTENTS

LIST OF FIGURES

LIST OF TABLES

NOMENCLATURE

NCE	New Chemical Entity
BCS	Biopharmaceutical Classification System
DMSO	Dimethyl Sulfoxide
PEG	Polyethelyne Glycol
G	Gibbs Free Energy
R	Universal Gas Constant
T	Absolute Temperature
σ	Saturation Solubility
σ_c	Saturation Solubility of the Crystalline Phase
σ_a	Saturation Solubility of the Amorphous Phase
a	Specific Surface Area
SA	Surface Area
m	Mass
d	Particle Diameter
ρ	Density
V	Volume
D	Diffusion Coefficient
h	Diffusion layer thickness
p	Vapor Pressure (functional)

p_0	Vapor Pressure (No Curvature)
V_m	Molar Volume
γ	Surface Tension
r	Droplet Radius
We	Weber Number
v	Velocity
l	Characteristic Length
Q	Flow Rate
ε	Electric Permittivity
ε_0	Electric Permittivity of Free Space
k	Electric Conductivity
κ	Evaporation Constant
t	Time
d_0	Initial Droplet Diameter
τ_D	Droplet Lifetime
Mw	Molecular Weight
IMC	Indomethacin
ϵ	Molar Absorptivity
b	Optical Path Length
A	Absorptivity
P	Luminous Intensity

CHAPTER 1: BIOAVAILABILITY AND SOLUBILITY

1.1 Pharmaceutical Research and Development Overview

The biopharmaceutical industry grosses over a trillion dollars annually (IMS 2012) and constantly expands via the discovery of new chemical entities. In order for these new drugs to become profitable and help people, they must pass FDA clinical trials as well as a preclinical battery. This process suffers from a substantial attrition rate demonstrated in Figure 1.

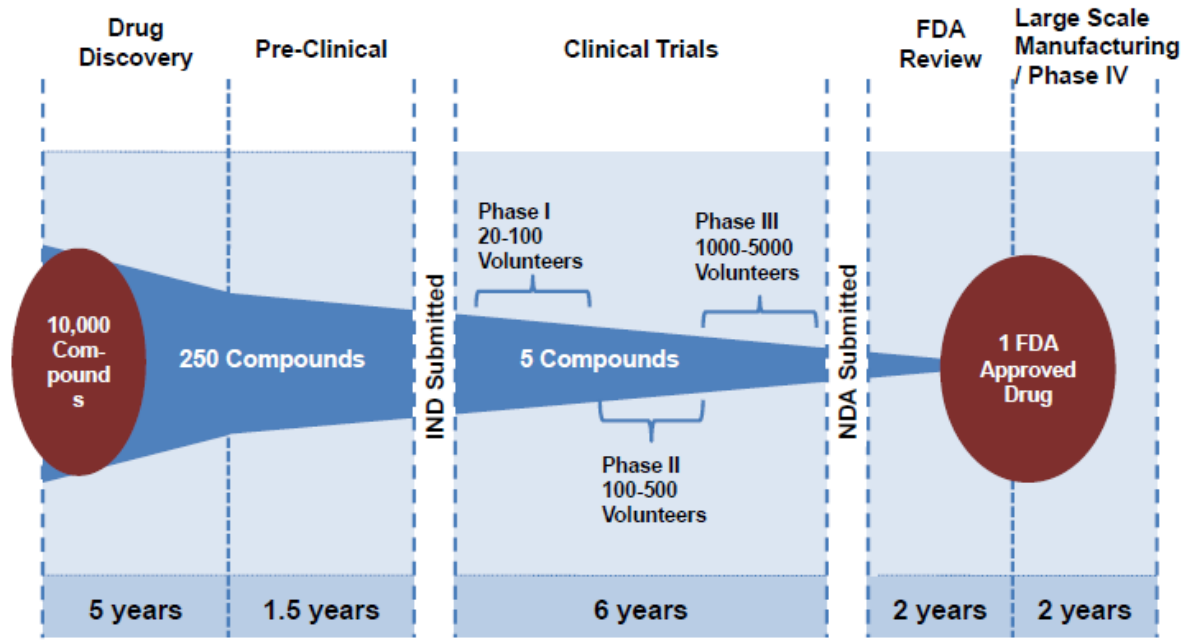

Quelle: Burrell Report Biotechnology Industry 2006

Figure 1: Attrition in the Pharmaceutical R&D Pipeline

Unfortunately for pharmaceutical developers, this attrition rate is only worsening with time. The issue is complex but owes some responsibility to screening processes and their effect on bioavailability.

1.1.1 Screening

Pharmaceutical research and development finds potential drug candidates through target based screening, phenotypic screening, modification of natural substances and biologic based approaches (Swinney et al, 2011). Most high potential chemicals come from the target based and phenotypic screening; these are high throughput, combinatorial processes. Target based screening allows for rational design of small molecule. This molecule design process finds chemical groups which react well with a certain target. Utilizing high throughput chemical libraries, these chemical groups find a suitable backbone yielding a final product. Phenotypic screening pushes high throughput screening to its limit; the process combinatorially tests vast libraries of chemicals until something meets the desired criterion. Since water tends to not facilitate chemical reactions as rigorously as these screening processes would prefer, dimethyl sulfoxide (DMSO) or polyethylene glycol (PEG) are almost always used as the solvent environment. (Babu, 2011) These non-aqueous environments of development can lead to unpredictable properties when exposed to an aqueous environment (such as the human body).

1.1.2 Biopharmaceutical Classification System

The Biopharmaceutical Classification System (BCS), pioneered by Amidon et al., specifically outlines how drugs can be classified and the system has been adopted widely throughout the industry. This system draws two qualifying lines of properties: solubility and permeability. Solubility, in this context, refers to the ratio between the saturation limit of a drug in water and the maximally effective dose. A non-dimensional constant is introduced to represent that number. Permeability is a measure of how well a chemical will pass through the body's biological boundaries and is measured by a partitioning constant. In the current state of biopharmaceutical research, good permeability comes readily from the screening process but solubility remains an elusive property for the pharmaceutical industry. With two independent quantities defining these chemicals, four classes naturally form from the different combinations of high and low solubility and permeability. Figure 2 demonstrates graphically the BCS and approximate distribution of current market and research and development drugs (Thayer et al.).

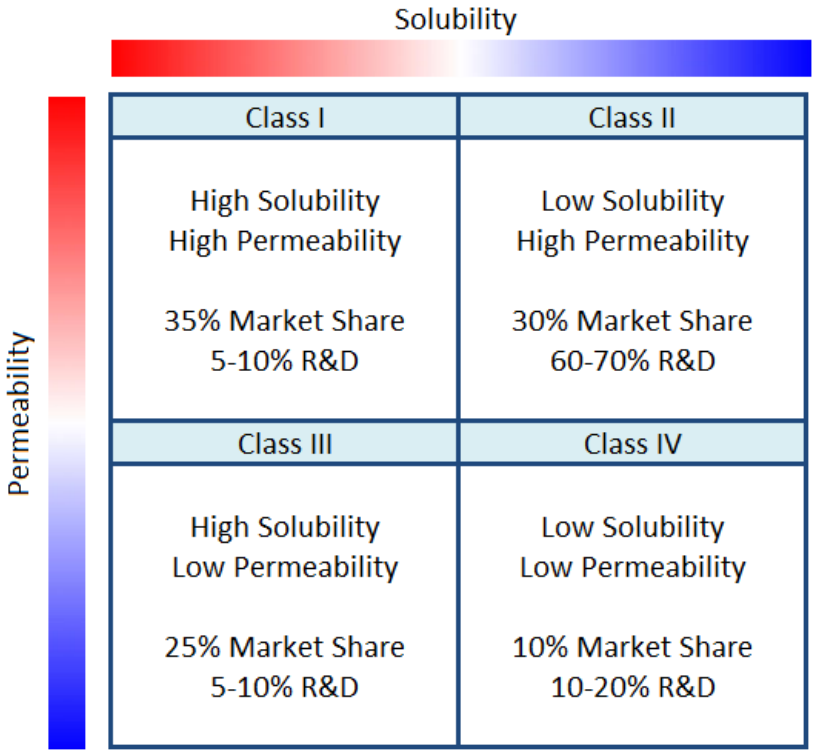

Figure 2: The BCS and Relative Distribution of Market and Research Drugs

1.1.3 Pharmacodynamics and Pharmacokinetics

Pharmacodynamics is the effect a drug has on the body. Target based screening focuses solely on the pharmacodynamics of a chemical. Tremendous resources are allocated in treating a symptom or specific efficacy criterion. Pharmacodynamics drives the entire innovation process within the pharmaceutical pipeline. Other critical properties also contribute to the success of a drug in the body.

Pharmacokinetics describes the absorption of the drug into the body, the distribution of the substance through the body, the metabolization of the chemical into waste product, and the excretion of those waste products safely out of the body. Those

four items constitute the ADME summary of pharmacokinetics. More generally, pharmacokinetics describes the body's effect on the drug i.e. how the body's systems handle it. Pharmacokinetic properties are determined by a host of factors but among the most important is the bioavailability of a compound, or the fraction of an administered dose that reaches the bloodstream. Bioavailability constitutes the first half of the pharmacokinetic story (absorption and distribution) and determines if and how a drug will act. Further, bioavailability strongly correlates with the qualities outlined in the BCS, solubility and permeability. Thus, while phenotypic and target based screening tackle the problem of pharmacodynamics, it is the solubility and permeability of a compound which largely indicate the pharmacokinetics.

1.2 Solubility

Because of the screening processes, many NCE products are designed without much thought into the pharmacokinetics and BCS properties. In fact, the unintended consequences of the high throughput screening are a shift towards high molecular weights and increasing lipophilicity. It has been reported that 40% of all marketed drugs are poorly water soluble. Further, between 70 and 90% of new chemical entities in the research pipeline suffer from low solubility (Thayer, 2010). It is widely accepted that tackling solubility issues in these drugs represents one of the largest challenges in drug development. Finally it is not enough to improve the saturation concentration but also

boost the dissolution rate since these chemicals have a limited amount of residence time in the digestive system.

This contribution focuses heavily on the improvement of solubility via processing of drugs (without chemical manipulation). To accomplish this effectively, parameters of solubility must be defined. First, the saturation limit of a chemical describes the highest concentration a solute will dissolve to inside a solution. This saturation limit is dependent on several things discussed in greater detail below. When boosting the solubility, supersaturation becomes a critical parameter. Supersaturation describes the ratio of the current concentration with the saturation limit of the chemical.

CHAPTER 2: THERMODYNAMIC AND DYNAMIC CONSIDERATIONS

After considering thermodynamics and molecular dynamics of the problem, an amorphous nanoparticle emerges as the prime candidate to augment solubility.

2.1 Thermodynamic Considerations

Dissolution is largely a thermodynamic phenomenon. A lower energy state in solution must coax each individual molecule from its solid bulk into a dissolved state. Successful dislodging of molecules relies on the outward force, here the dissolution pressure, to overwhelm the attractive forces of the solid state. These include all manner of intermolecular forces including dipole forces or van der Waals forces. To improve both saturation solubility and dissolution rate, these forces must reach minimum. These may be analyzed in bulk by use of enthalpy and Gibbs 'Free Energy.' A solid with higher free energy and enthalpy is expected to have more favorable thermodynamic properties, including solubility (Hancock, Zografi 1997).

2.1.1 Solid State

The energy associated with a solid depends greatly on its solid state. Many, if not most, solids may exist as several different polymorphs. Many of these polymorph arrangements involve merely changing the crystal lattice arrangement. Long range order, in general, indicates a stable state with energy sunk into the crystalline order. The amorphous solid state describes a solid state wherein molecules exhibit no long range

order. This solid state has no crystal lattice; the atoms are merely jumbled together. This solid state has the highest free energy of all solid states. Consequently it also displays the most extreme thermodynamic properties. Figure 3 shows the Free Energy advantage of the amorphous solid state (there called a glass) over its crystalline counterparts.

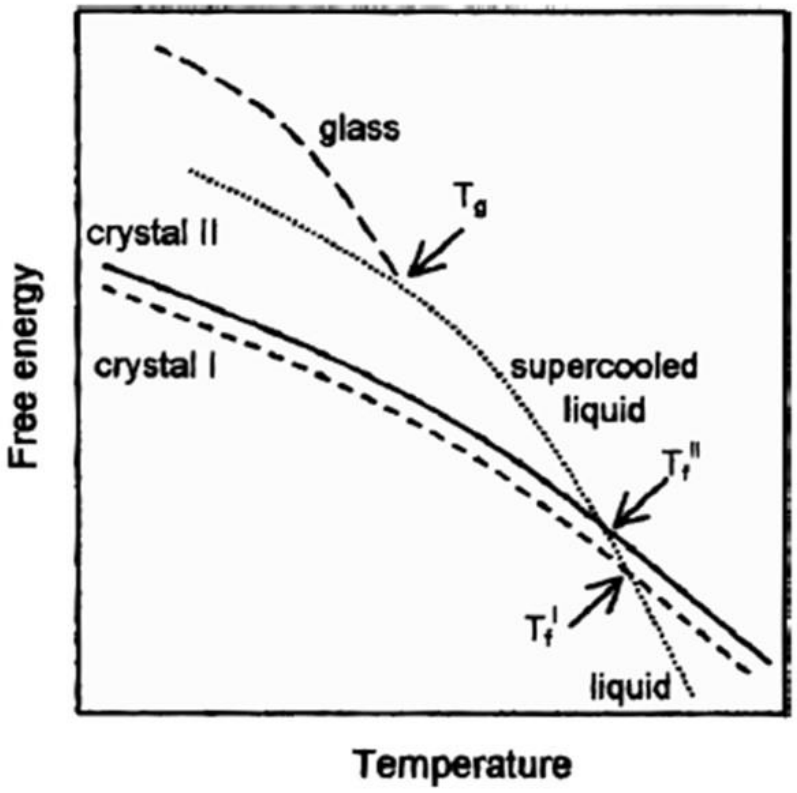

Figure 3: Characteristic Free Energy-Temperature Diagram for an Arbitrary Chemical

2.1.2 Amorphous Characteristics

The traditional formation of amorphous solids involves cooling. When cooled below its freezing point, a material tends to crystallize into a solid. By preventing that mechanism, the material enters a 'supercooled' liquid phase. In this phase, molecular mobility begins to diminish along, accompanying a rising viscosity. At another critical

temperature, called the glass transition temperature, this viscosity spikes and the material becomes practically frozen in a disordered state. Figure 4 shows the change in the arrangement between an ordered crystal lattice and the jumbled, disordered amorphous state.

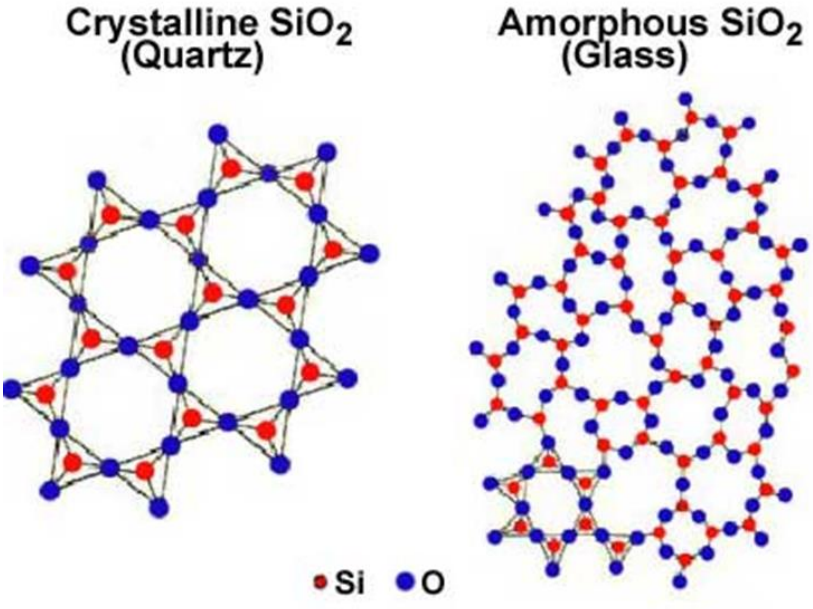

Figure 4: Crystal Lattice vs. Amorphous Solid Example

In many cases, time scales of solidification interrupt the crystallization process. For example, the rapid cooling of a melt often outpaces the crystallization process. Another example in which we take great interest involves the rapid precipitation from solution (Hancock, Zografi 1997).

2.1.3 Amorphous Solubility Advantage

Hancock and Parks have done extensive work in evaluating a solubility advantage of amorphous solids. This study chose Indomethacin for detailed examination but also

examined several other drugs for somewhat less detailed analysis. The amorphous state of the studied drugs were obtained via quench cooling of molten material. They were then compared with the crystalline forms of that drug.

2.1.3.1 Theoretical

In the above referenced work, they predict the solubility advantage with a quite simplified free energy model. Parks and co-workers (Parks 1928, 1934) developed this model for the solubility advantage of amorphous chemicals.

$$\Delta G = -RTln\left(\frac{\sigma_a}{\sigma_c}\right) \quad (1)$$

Clearly, this model predicts that higher free energy yields a much higher solubility ratio. This simple model approaches the amorphous solid state as a pseudo-equilibrium solid state at all temperatures below the glass transition temperature. Since the amorphous state has the highest possible free energy, it should also be most soluble. Almost astonishingly, this model predicted the solubility of the amorphous chemicals to fit anywhere from 12 to 1652 times the solubility of the crystalline form.

2.1.3.2 Experimental

The experimental data in this study aligns well qualitatively but departs quantitatively from the free energy model. In the case of Indomethacin, the solubility ratio was predicted between 25 and 104 but the measured solubility ratio was 4.5 at room temperature. The dissolution profile at room temperature is presented in Figure 5.

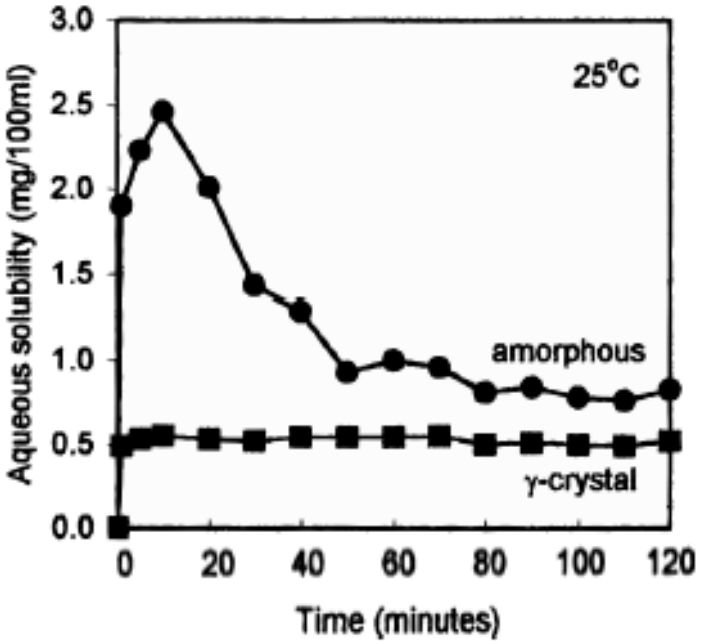

Figure 5: Dissolution Profile of Amorphous and Crystalline IMC at 25 Degrees Celsius

There are some important things to note about the dissolution profile in Figure 5. First, the concentration of the crystalline substance appears to quickly rise to its saturation limit as predicted. In the amorphous case, a sharp peak occurs to the maximum solubility limit. The saturation then meanders down to a 'steady state' concentration (much less than the peak). The presented solubility ratio refers to the drastic peak rather than the steady condition. Even the presented solubility ratio falls far short of the predicted value.

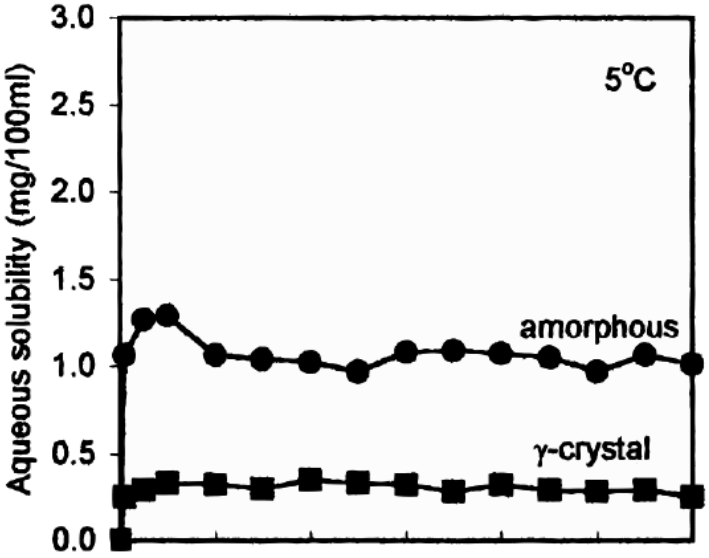

Figure 6: Dissolution Profile of Amorphous and Crystalline IMC at 5 Degrees Celsius

For comparison, the dissolution profile at 5°C is presented in Figure 6. In contrast to Figure 5, at this cooler temperature the saturation peak seems far less drastic and the steady state condition maintains a larger solubility gap. At this cooler temperature, the predicted solubility ratio was higher than at room temperature, stated as 38-301. The measured solubility ratio was 4.4.

2.1.3.3 Discrepancy

The tremendous quantitative discrepancy between theoretical and experimental data attributes to the incompleteness of the model. An explanation presented by Hancock and Parks derives from the strong recrystallization force from a supersaturated medium. Regardless of this precipitative trend, the qualitative solubility advantage is undeniable. A quadrupling of solubility significantly impacts the possibility of moving a drug from a Class II drug to a Class I drug.

2.2 Dynamics

The dynamics of dissolution and solubility stand on the pillars of surface area and particle curvature. Both of these properties depend strongly on particle size and shape.

2.2.1 Surface Area

When discussing surface area, a critical step involves fixing the amount of mass. In a pharmaceutical sense this manifests as the dosage level. It therefore becomes useful to utilize specific surface area, or the ratio of surface area to mass. This relationship states

$$a = \frac{SA}{m} = \frac{SA}{\rho V}. \tag{2}$$

Naturally, when density is held fixed this relationship becomes the ratio of surface area to volume. If one considers a spherical particle, then this relationship may become simplified. Hence,

$$a \propto \frac{SA}{V} = \frac{\frac{\pi}{4}d^2}{\frac{\pi}{12}d^3} = 3d^{-1}. \tag{3}$$

Equation 3 yields the result that given a certain amount of mass to break into spherical particles, surface area increases monotonically (and asymptotically) as diameter shrinks.

2.2.2 Dissolution Rate

Dissolution rate experienced great growth in understanding in the early part of the 20th century. First, Noyes and Whitney in 1897 proposed that the dissolution rate was proportional to the difference between the concentration of the solution and the

saturation concentration. Brunner and Tolloczko made another leap in 1900 by proposing that dissolution rate also scaled directly with surface area. That the dissolution rate scales with exposed area provides a convenient method to improve the dissolution rate. Finally Nernst and Brunner included the conclusions of Fick's second law into the dissolution rate in 1904, finding that dissolution rate was inversely proportional to the diffusion layer thickness. All told, the statement of a fully evolved Noyes-Whitney equation is presented in Equation 4.

$$\frac{dc}{dt} = \frac{DS(\sigma - c)}{h} \tag{4}$$

2.2.3 Curvature Effects

For most cases, saturation solubility is constant for a given material. This relationship maintains validity for all sizes until a critical particle size of 1-2 μm below which saturation solubility becomes functionally dependent on size. It becomes apparent at these small sizes that as particle size decreases, saturation solubility increases (Junghanns and Muller 2008). The reasoning behind this phenomenon relies on the curvature of submerged particles.

When considering the effect of curvature on solubility, important analogies must form. According to Junghanns and Muller (2008), "The situation of a transfer of molecules from a liquid phase (droplet) to a gas phase is in principal identical to the transfer of molecules from a solid phase (nanocrystal) to a liquid phase (dispersion medium). The vapor pressure is equivalent to the dissolution pressure." With this analogy in place,

properties of vaporization apply analogously to dissolution. Importantly, increasing dissolution pressure also increases equilibrium solubility.

An important relation in the world of vaporizing droplets (and in dissolving particles) comes from the Kelvin equation, stated below. This equation demonstrates a tremendous rate of increase in vapor pressure with radius tending to zero but relatively small effects for relatively large radii.

$$p = p_0 \exp\left(\frac{2\gamma V_m}{rRT}\right) \tag{5}$$

The Kelvin equation, coupled with the analogy between dissolution and vaporization explains the dependence of saturation limit on particle size.

CHAPTER 3: ATOMIZATION AND EVAPORATION

3.1 Electrospray

Electrospray describes one method of atomizing a liquid into a field of droplets. This method attracts interest for three primary benefits. First, electrospray produces primary droplets which are monodisperse, or have small variation in size within the droplet population. Second, tuning experimental parameters allows for enormous variation in mean droplet diameters, ranging from hundreds of microns down to mere nanometers. Finally, these desirable droplet characteristics emerge without dependence on the initial size of the nozzle allowing for large nozzles and minimal clogging.

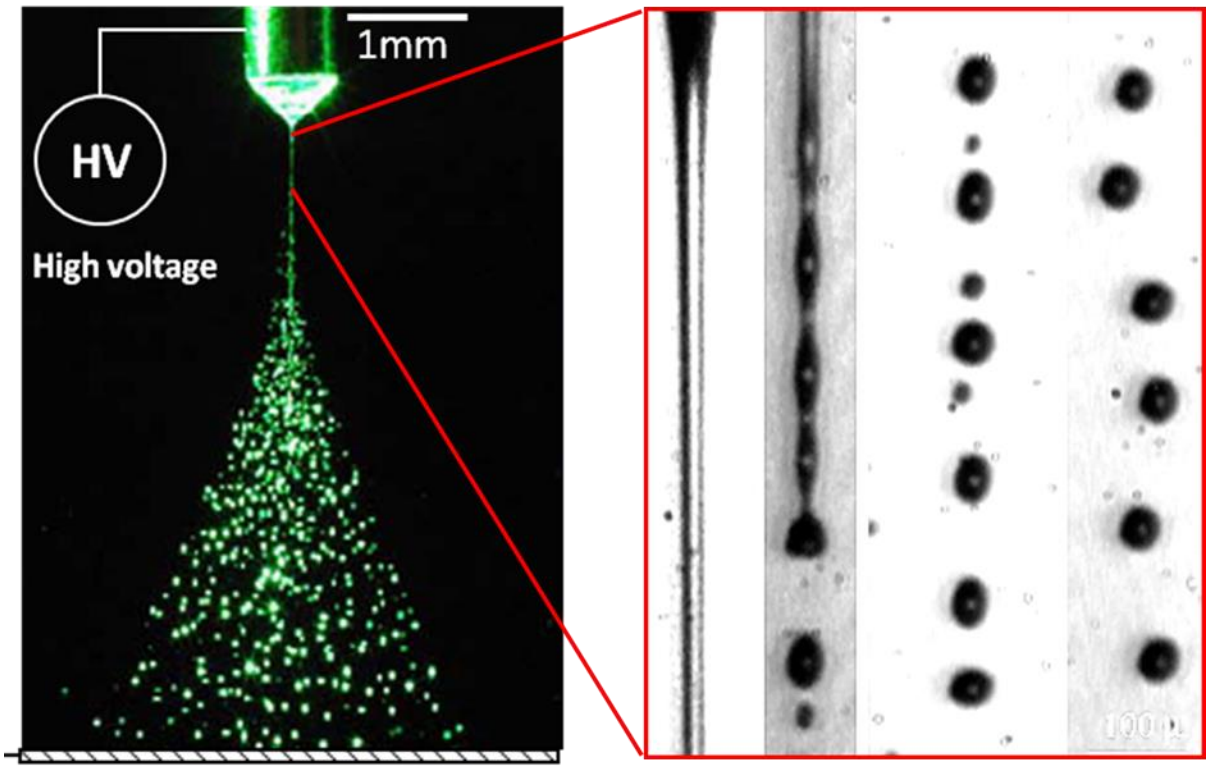

Figure 7: Left: Stable Taylor Cone and ES Shroud; Right: Schematic of Jet Breakup

The mechanism of electrospray uniquely relies on electro-hydrodynamic forces and their interplay with surface tension. A brief overview of uncharged spray like phenomena (hereon referred to as ballistic emission) aids the natural implementation of electrostatic effects.

3.1.1 Ballistic Jet

Consider a hollow rigid column with an end exposed to the environment (a nozzle) and liquid flowing toward the exposed end. One expects this liquid, once ejected from the nozzle, to form a column of liquid on the basis of inertia (note: inertia generally scales with density, ρ, and the square of velocity, v. This expectation decomposes as

inertia decreases with diminishing flow rate. In fact, surface tension ($\gamma, \frac{N}{m}$) quickly dominates the behavior of this liquid as inertial values decrease. The relative magnitudes of inertial forces are compared with surface tension forces in the dimensionless Weber number (equation 6) and frequently appears in the analysis of liquid jets, jet breakup, and aerosol science at large.

$$We = \frac{\rho v^2 l}{\gamma} \tag{6}$$

The competition between surface tension and inertia in ballistic emission results in two distinct modes of operation: dripping and jetting. While technical descriptions of these modes exist, a more direct understanding evolves from example. Any household faucet operates in the jetting mode during full use but experiences the dripping mode during much smaller flow rates.

3.1.2 Electrospray Jet

Electrospray throws another hat in the ring of this match between inertia and surface tension. Consider further a high voltage applied between the previously described nozzle (with the added condition that the nozzle conduct electricity) and a grounded plane some distance away. This high voltage creates an electric field between the nozzle and the ground. Charge carriers within the fluid feel a force from exposure to this field, generally directed toward the ground. This force competes directly with surface tension forces.

3.1.3 Solution

The above description heavily simplifies the process and serves only to yield an intuitive understanding of the phenomenon. In fact, electrospray relies on a complex array of factors including the precise geometry of the electric field, supplied fluid flow rate, nozzle diameter, and especially solution properties. Among the solution properties, some of the most critical to the process are surface tension γ, viscosity μ, electrical conductivity k, and the dielectric constant ε (Almeria 2010). The rather intensive influence on solution properties implies the necessity of appropriate planning in the production of ink. Experimental parameters to be adjusted then become flow rate and voltage.

3.1.4 Stability

This competition results mostly in chaos; the exposed liquid rapidly oscillates between states of surface tension and electrostatic domination. There exists a small region of stability within the control parameters where this chaos subsides and a stable solution emerges. This solution involves a linear drawdown in diameter of the exposed jet until the diameter reaches some small fraction of the original diameter of the nozzle. Once the diameter shrinks to the characteristic value, an incredibly small jet emerges. The name 'Taylor Cone' refers to this stable island and represents the preferred mode of operation for electrospray.

As previously mentioned, the Taylor Cone operates at a small island of parameters. More practically, for a given solution, only a certain range of flow rates may

sustain a stable cone-jet mode of emission and that Taylor Cone appears between two voltage values. This carves a domain space out of the Flow Rate – Voltage Plane within which we expect stable operation. This domain space changes drastically between different solutions (on the basis of solution characteristics).

3.1.5 Droplets

The field of droplets in electrospray also exhibit interesting phenomena. The droplets contain a charge due to the electric potential. This charge leads to interesting divergence from the ballistic case.

Again for comparison, consider the ballistic case. If operating in a jetting mode, then the column of liquid will propagate through the environment. The instability of this jet causes it to decompose into a series of droplets (Rayleigh). These droplets then proceed along their path subject only to outside forces such as gravity. Without external methods of distributing these droplets over an area, they simply stack at their ballistic target.

The case of charged droplets diverges significantly from the ballistic case. The small jet erupting from the tip of the Taylor Cone still decomposes into droplets as expected. These droplets, however, are strictly bimodal and contain charge. The jet breaks into two types of droplets: larger primary droplets and smaller satellite droplets. The intrinsic charge in each droplet repels each other droplet by traditional Coulombic repulsion (since they are all of like-charge). The smaller droplets feel a greater acceleration (owing to the smaller mass) and repel to an outer shroud. The primary

droplets remain in the core of the droplet cloud. These primary droplets exhibit the best monodispersity (~10% RSD). Even these primary droplets remain at the relative core of the cloud of droplets, the electrostatic repulsion self-disperses the droplets over an area here called the footprint of the spray.

The size of these droplets, often the defining desirable result of electrospray, generates healthy interest. Though many models and scaling laws exist, the most common was proposed by de la Mora and Loscertales (1994). Droplet diameter scaling with the cube root of flow rate is the most significant takeaway, but the formula is shown below.

$$d = G(\varepsilon)\left(\frac{Q\varepsilon\varepsilon_0}{k}\right)^{\frac{1}{3}} \tag{7}$$

where $G(\varepsilon)$ is a function of unity order.

3.1.6 Multiplexing

The impetus for multiplexing electrosprays is simple. A single cone jet operates at flow rates of liters per year while industrial standards command liters per minute. The only way to attain such a massive scale up while maintaining the quality of electrospray desired lies in multiplicity. If the number of nozzles may increase without bound, then any throughput requirement may be met. Since cost of manufacturing nozzles scales with area manufactured, cost per nozzle naturally decreases with improved packing density (Deng, 2009). Increasing packing density can be attained through reduction of nozzle size. Smaller nozzle sizes minimize the amount of solvent which evaporates from the

meniscus, thus minimizing the cost of recovering or losing that solvent. Further, augmented packing density improves the homogeneity of the electrospray cloud thus improving performance per nozzle or per apparatus. Deng et al. (2006, 2009) has demonstrated some of the best packing densities for area coverage as shown in Figure 8.

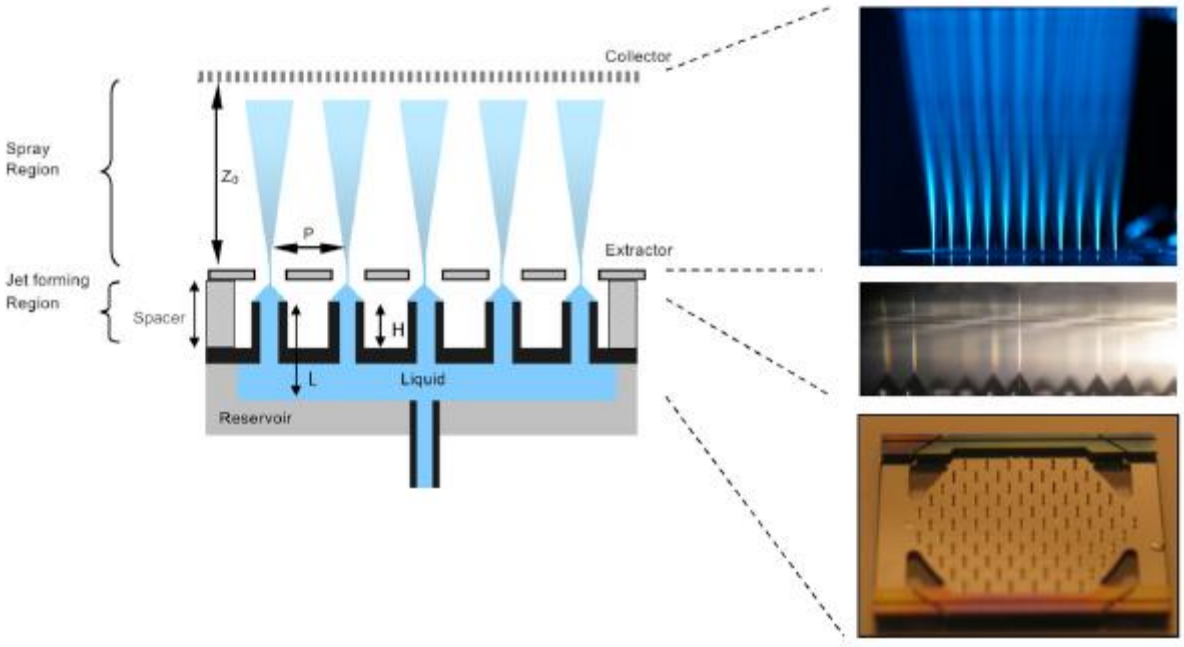

Figure 8: Multiplexing Device with Hexagonally Distributed Nozzles (Deng, 2009)

Another multiplexing method is the linear array where nozzles are not arranged throughout an area but rather in a line. Linear packing yields cheap and compact nozzle arrays without suffering from losses in homogeneity (Lojewski et al, 2013). This spatial compactness is well suited for many manufacturing processes, especially the so called roll-to-roll method where the product is in motion. This motion can effectively eliminate

the requirement for two dimensional depositors in order to produce two dimensional depositions.

3.2 Evaporation

When producing particles via spray drying, evaporation plays a central role. With respect to the production of amorphous nanoparticles and the maximization of surface area, the critical effects of evaporation are droplet lifetime and particle morphology.

3.2.1 Droplet Lifetime

Though only a simplified model of evaporation, the d^2 model of droplet evaporation suitably covers most cases of small molecule solutions. The d^2 model states

$$d^2(t) = d_0^2 - \kappa t. \tag{8}$$

Thus, in a droplet, the surface area decreases linearly with time. An important consequence of this law is the droplet lifetime,

$$\tau_D = \frac{d_0^2}{\kappa}. \tag{9}$$

Hence, smaller droplets have much shorter lifetimes than large droplets.

3.2.2 Frustration of Crystallization

To produce an amorphous solid by precipitation out of solution, nucleation must vastly outpace crystal growth (Mullin 2001). Further, the crystal growth rate is bounded linearly by the supersaturation of the solvent by the Burton-Cabrera-Frank supersaturation growth relationship. Further, the classical model of nucleation proposed

by Volmer in 1925 yields precedent for a highly nonlinear (and accelerative) relationship between nucleation and supersaturation. Thus as supersaturation increases, nucleation becomes the dominant phenomenon. The degree of amorphicity relies heavily on this supersaturation in solution. The specific relationship between the two and any optimization which might occur is beyond this contribution. We simply conclude that as the droplet diameter decreases (and droplet lifetime) that the metastable supersaturation will increase thus increasing the nucleation rate relative to crystal growth. Since the evaporation rate of solvent also effects the droplet lifetime, increasing the volatility of solvent will also augment the nucleation rate relative to crystal growth.

CHAPTER 4: EXPERIMENTAL APPROACH AND VALIDATION

In this contribution, we propose electrospray as a production method for amorphous nanoparticles of poorly soluble therapeutic agents. Electrospray demonstrates necessary qualities for the process including a capacity to produce very small droplets and flexibility to many conducting solvents. Two other properties elevate electrospray's alignment within the pharmaceutical field: scalability and monodispersity. The expansion of multiplexing by Deng and others have propelled electrospray into low cost scale up to any industrial need. Further, the uncommon property of monodispersity dramatically increases reproducibility, minimizing batch to batch variation.

A model drug is chosen to represent many Class II drugs. A solvent which may dissolve the model drug and fit well with electrospray forms the solution headed to further analysis. Four properties need evaluation: size, shape, crystallinity, and solubility profile. Scanning Electron Microscopy evaluates the morphology of the particles. X-Ray diffraction reveals sample crystallinity. Finally, UV-Vis Spectroscopy is utilized to form a dissolution profile (concentration over time) to evaluate a real solubility advantage. Each of these three methods of analysis require different experimental parameters discussed in detail below.

4.1 Model Drug

Indomethacin (IMC), a hydrophobic and poorly water soluble drug, represents an ideal chemical for study because literature has already explored this substance with great zeal (Babu and Nangia 2011; Andronis et al 1996; BASF 2011; Hancock Zografi 1996; Jain 2000; Hancock and Parks, 2000; Hernandez et al, 2008; Yamamoto 2012). The chemical structure of IMC is shown in Figure 9.

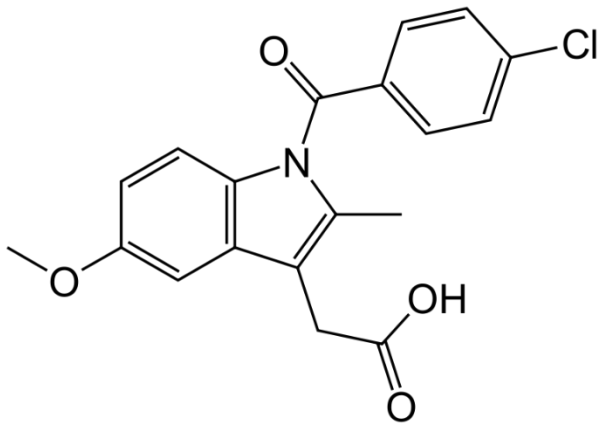

Figure 9: Molecular Structure of Indomethacin

Of course, properties of the IMC will be critical to its analysis. The relevant properties are presented in Table 1. The indomethacin in this study was acquired from sigma Aldrich at >99% purity.

Table 1: Properties of Indomethacin

Indomethacin Properties		
Property	Value	Unit
Molecular weight	358	$g \cdot mol^{-1}$
Aqueous Solubility	0.937	$mg \cdot L^{-1}$
Melting Point	438	K
Glass Transition	320	K
ρ (crystalline)	1.38	$kg \cdot m^{-3}$
ρ (amorphous)	1.32	$kg \cdot m^{-3}$
Absorption Peaks	260, 319	nm

4.2 Solvent choice and Solution Properties

Electing a solvent for processing presents a deal of complexity, especially when involving electrospray. First and foremost, this solvent will need to dissolve IMC. It must have favorable characteristics for electrospray. If those conditions are met, then things such as cost and toxicity may influence the decision.

Indomethacin, though practically insoluble in water, shows reasonable solubility in ethanol, the ethers, acetone, castor oil, and chlorinated solvents. Castor oil and the chlorinated solvents tend to perform poorly as electrospray feed. Acetone and ethanol are more polar than many of the ethers. Between acetone and ethanol, neither is superior for electrospray. Acetone shows further promise in the production of amorphous particles due to the high volatility of acetone. This decreases the droplet

lifetime. Because of this, acetone is used for the solvent in the electrospray feed. The relevant properties of acetone are presented in Table 2.

Table 2: Properties of Acetone

Acetone Properties		
Property	Value	Unit
Molecular Weight	58	$g \cdot mol^{-1}$
Boiling Point	177.65	K
Vapor Pressure	24	kPa
Density	791	$kg \cdot m^{-3}$
Vapor Density (Air=1)	2	-

4.3 Experimental Procedure

First a solution of indomethacin and acetone was made. In these experiments a solution of 1.5%wt indomethacin was used. The solution is then loaded into a 9.5 mm diameter syringe and loaded into a Model NE-300 New Era Pump Systems Inc. syringe pump operating at 12 V and .75A. The flow rate needs to minimize for the smallest droplet possible. While a stable cone could not be held indefinitely at 100 microliters per hour, 150 microliters per hour showed indefinite stability. The nozzle used was a 250 μm ball tip of a ball point pen. This pen tip serves the same function as a hollow nozzle though exhibits a larger stability island due to the viscous impedance created by the ball. Similarly, a flat tipped hollow nozzle could have been used. The working distance between the nozzle and substrate was chosen to be excessively large such that the

droplets were guaranteed to fully dry by the impact time. The droplet lifetime of a $5\mu m$ droplet of acetone (evaporation constant of $2 * 10^{-8}\frac{m^2}{s}$) will be $\tau_D = \frac{(5*10^{-6}m)^2}{2*10^{-8}} \approx 1ms$ Overestimating the steady droplet speed as $10\frac{m}{s}$, the distance a droplet should require for full evaporation is roughly 1 cm. For these trials, a working distance of no less than 4 cm were used. The stability voltage varied for each trial, but a voltage was consistently chosen between 1 and 10 kV. This value mostly comes as a result of the other parameters and is set merely to achieve stability. Each experiment presents the full array of experimental parameters which accompany that run.

4.4 Morphological Studies

Although the applicable product to the pharmaceutical industry is powder, all samples in this study were deposited onto some substrate. For analysis under scanning electron microscopy, samples were deposited on copper coated silicon wafers. Because IMC may not conduct electricity, all samples underwent a sputter coat of gold and platinum for 90 seconds. First, several single layer deposition of particles allowed for sizing analysis of individual particles. Then, an increased exposure time sample elucidated an interesting development.

4.4.1 Crystalline Indomethacin

When seeing the micrographs of deposited Indomethacin, a crystalline reference state is useful. Figure 10 shows the morphology of the crystalline indomethacin purchased from Sigma Aldrich.

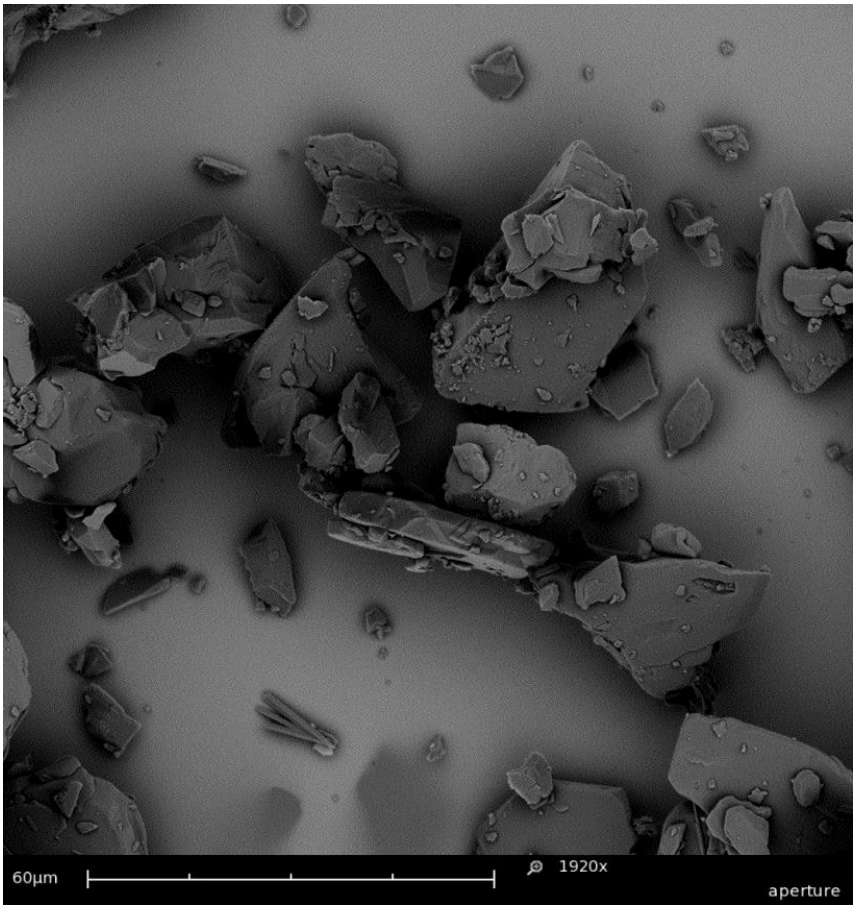

Figure 10: Micrograph of Crystalline Indomethacin

4.4.2 Monolayer Deposition

4.4.2.1 Flow Rate Dependence

Recall that the droplet size of electrospray is proportional to the cube root of flow rate. Because we desire small droplets, minimal flow rate is necessary. To verify the cube root dependence, IMC was spray deposited twice: once at a flow rate of 150 microliters per hour and once at 8 times that flow rate. The precise experimental parameters given in Table 3.

Table 3: Experimental Parameters of a Slow Flow Rate Spray (left) and Higher Flow Rate (right)

Experimental Parameters		
Solvent	Acetone	Mw= 58
Solute	IMC	Mw= 358
Flow Rate	0.15	mL/h
Concentration	1.5	%wt
Exposure Time	5	min
Footprint Diameter	6	cm
Working Distance	6	cm
Voltage	6.2	kV
Date	2/19/2014	

Experimental Parameters		
Solvent	Acetone	Mw= 58
Solute	IMC	Mw= 358
Flow Rate	1.2	mL/h
Concentration	1.5	%wt
Exposure Time	5	min
Footprint Diameter	12	cm
Working Distance	6	cm
Voltage	6.57	kV
Date	2/19/2014	

The resulting morphologies are given in Figures 11 and 12. By inspection, it is clear that the scaling law holds generally. In this deposition, the particles are morphologically odd in the case of smaller flow rates but more spherical in the larger flow rate case. This modulation of morphology is not unimportant as all deviation from a sphere increases specific surface area.

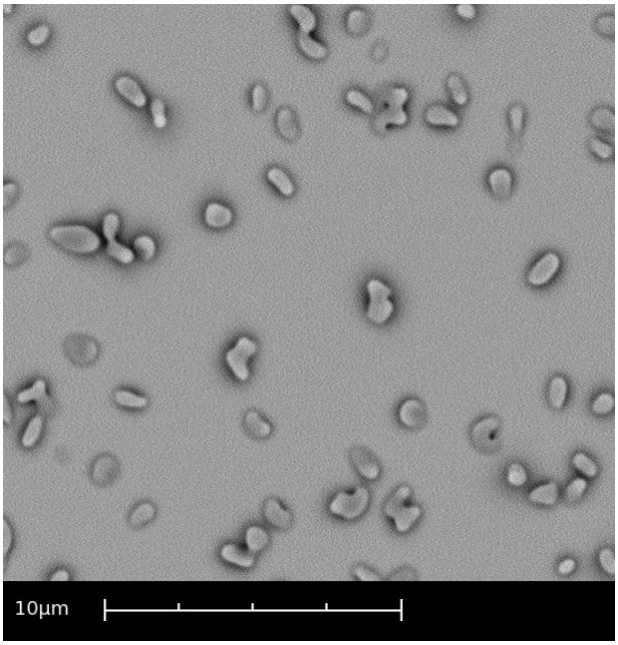

Figure 11: Micrograph of Slow Flow Rate Deposition

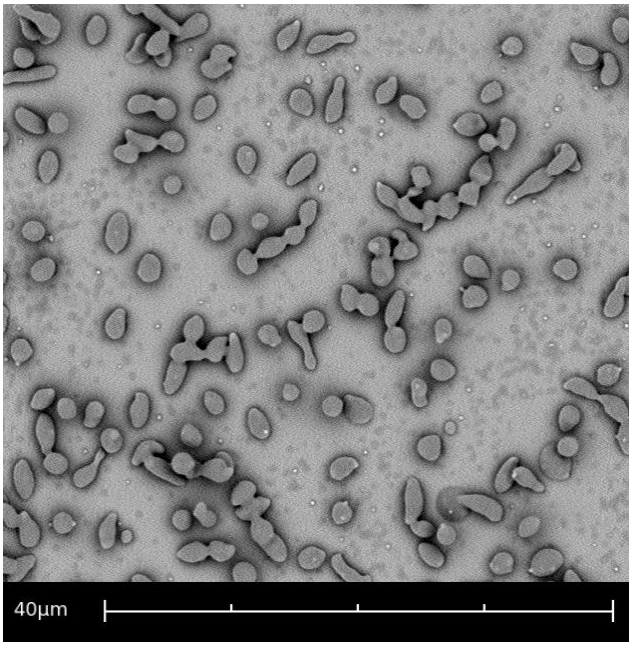

Figure 12: Micrograph of Higher Flow Rate Deposition

4.4.2.2 Sizing Study

In this monolayer deposition study, the experimental apparatus deposited a solution of IMC for a short time to gather a single layer of particles. The experimental parameters are collected in Table 4. A flow rate of 150 microliters per hour is the smallest flow rate that a stable cone could be generated with the experimental apparatus described above.

Table 4: Experimental Parameters of the Sizing Study

Experimental Parameters		
Solvent	Acetone	Mw= 58
Solute	IMC	Mw= 358
Flow Rate	0.15	mL/h
Concentration	1.5	%wt
Exposure Time	0.5	min
Footprint Diameter	2.5	cm
Working Distance	4	cm
Voltage	4.88	kV
Date	1/7/2013	

This sample was examined under a Phenom SEM and several pictures were taken at 7750x magnification. One such image is shown in Figure 13**.** The particles formed morphologically as dimpled spheres.

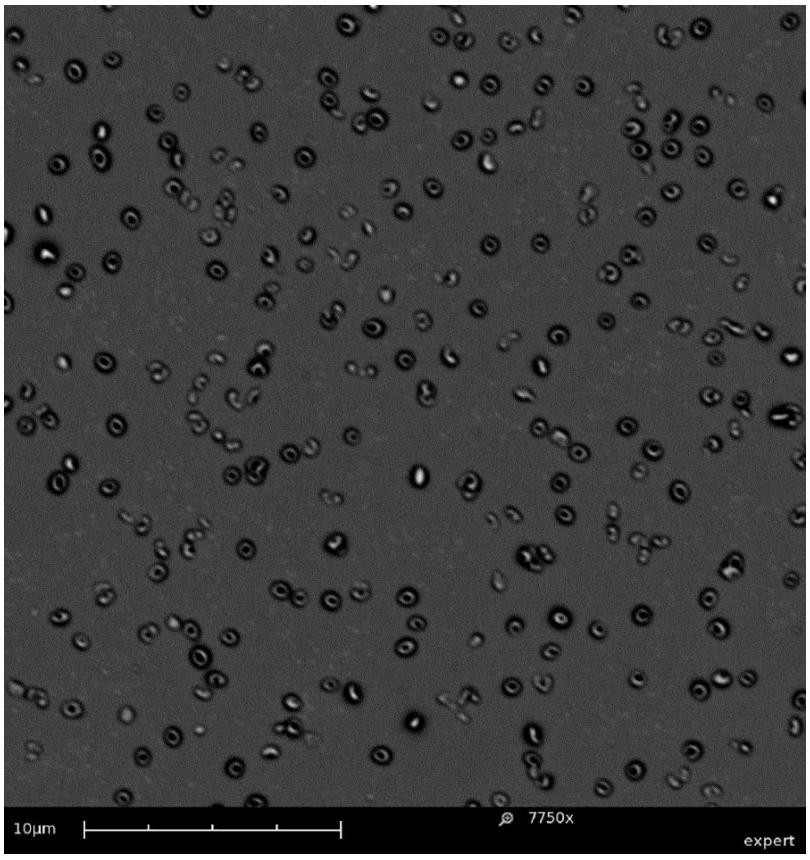

Figure 13: Micrograph of the Deposition Used for Sizing

These images were then analyzed in ImageJ image analysis software (NIH) for the size distribution of the particles. The results from this size distribution are presented in Table 5. Even with a reasonably high sample population, the relative standard deviation remains below 30%.

Table 5 Resutls of the Sizing Study

Results		
Number of Particles	Average Diameter (micron)	St. Dev (micron)
516	0.64	0.18

4.4.3 Multilayer Deposition

In later trials, a larger volume than a single layer becomes necessary for analysis. To gauge the type of matrix formed by layers of these particles, low weight solution of IMC in acetone was spray deposited for an extended time span. The experimental parameters for this specific deposition are shown in Table 6.

Table 6: Experimental Parameters of a multilayer deposition

Experimental Parameters		
Solvent	Acetone	Mw= 58
Solute	IMC	Mw= 358
Flow Rate	0.15	mL/h
Concentration	1.5	%wt
Exposure Time	120	min
Working Distance	6	cm
Voltage	6.03	kV
Date	1/3/2014	

Figure 14 shows the resulting particle matrix. Interestingly, the powder does not appear as a stack of spheres as one would expect of a powder, but rather an interconnected matrix with some degree of continuity. The matrix still tends to bulge as if retaining memory of its constituent particles but does not appear to be dispersed. That being said, the branches apparent in Figure 14 are of characteristic length consistent with the sizing study; the thicker bulges average in the 700 nanometer range with a tolerance of roughly 200 nanometers. The 'necked' narrower regions may reach dimension as small as 100 nm.

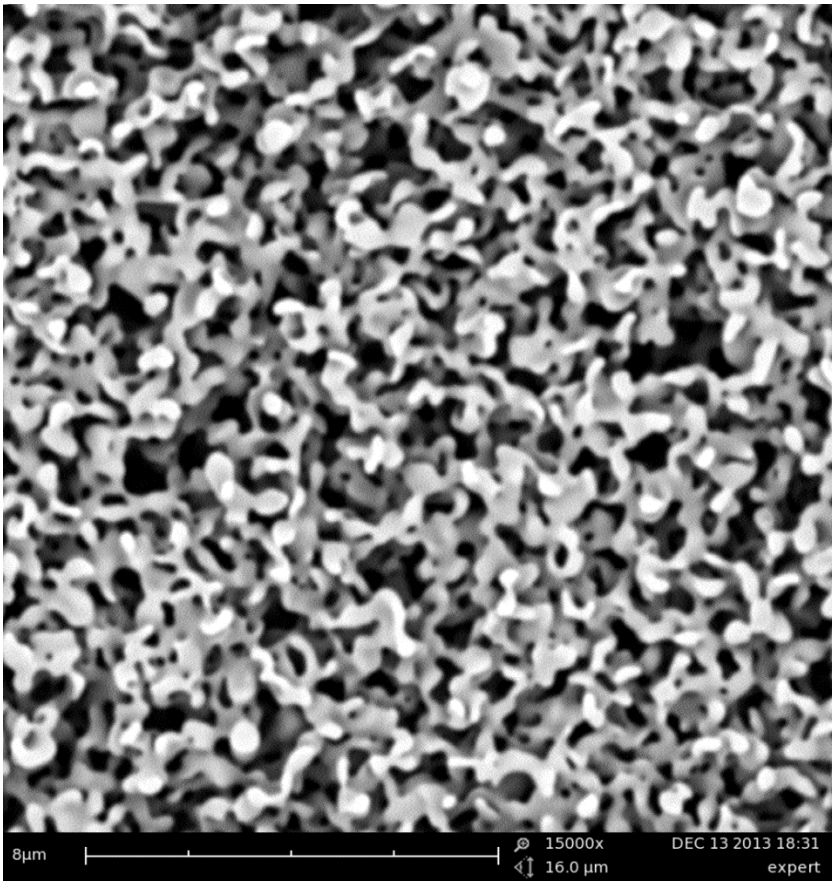

Figure 14: Micrograph of Layered Depostion

4.5 Crystallinity Evaluation

To evaluate the amorphicity of the deposited indomethacin, X-Ray Diffraction will be used. Deposited particles only reach thicknesses <10 μm during reasonable experimental time scales, so Thin Film X-Ray Diffraction is utilized for evaluation.

4.5.1 Literature

Hernandez et. al. performed X-Ray Diffraction on two different polymorphs of Indomethacin as well as the amorphous state. A Siemens Kristalloflex 5000 diffractometer

was used. Their data are presented in Figure 15. Curve C represents the diffraction pattern of the γ crystal, curve B shows the α crystal, and curve A is amorphous.

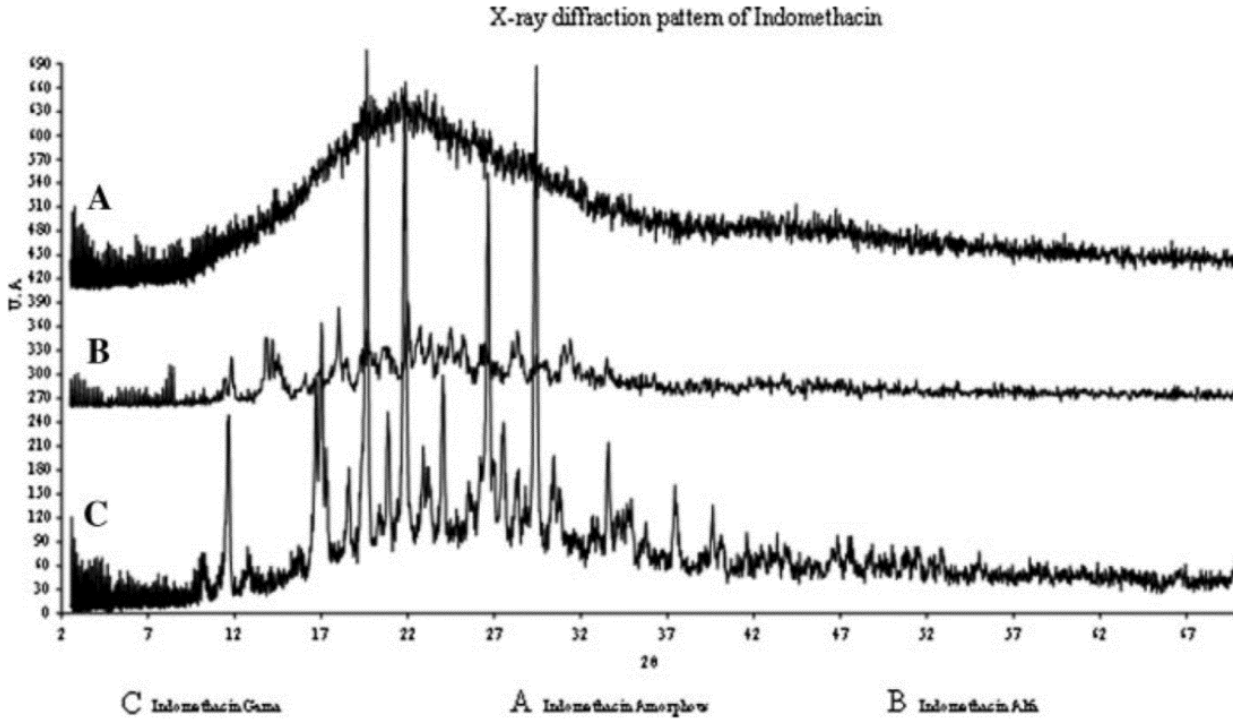

Figure 15: X Ray Diffraction of Indomethacin in Various Forms from Literature

4.5.2 Experimental

For crystallinity evaluation of electrospray deposited particles, X-ray diffraction was performed on a Rigaku D/MAX XRD with a 40kV Copper X-ray tube, 2 Theta Goiniometer, Datascan 4 Acquisition Software, and a thin film diffraction attachment. Both a crystalline sample and amorphous sample were analyzed. Figure 16 shows both curves gathered on the same axes. 2θ spanned 10-40 degrees. The incident angle was held constant at 5 degrees. Because IMC is an organic molecule, diffraction is expected only at lower angles; this is supported by literature (Hernadez et al).

The diffracted sample used the standard solution of this study (1.5%wt, .15 mL/h) with a sample exposure time of 60 minutes. This elongated exposure time allows the sample to obtain a sufficiently thick coating for analysis. At this time, the thickness of the film is underestimated to be on the order of the diameter of the particles. This guarantees at least a monolayer thickness, particularly at the core of the spray. Figure 16 shows the diffraction data of the amorphous sample (quite flat and blue) superposed over the diffraction data for the crystalline powder (substantially higher peaks and red).

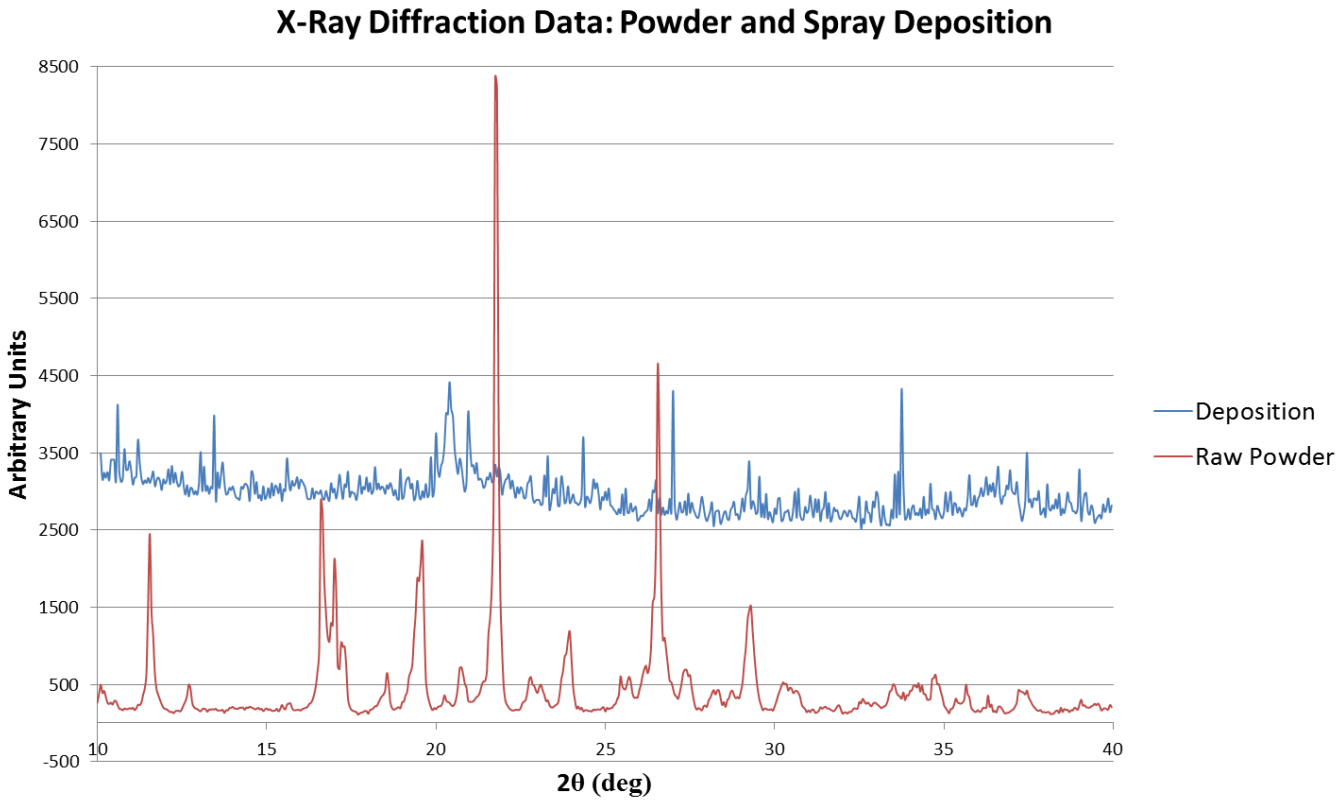

Figure 16: Experimental X-ray Diffraction of Amorphous and Crystalline IMC

The data demonstrates strong agreement with literature. We conclude that spray dried IMC lacks crystalline structure, as predicted.

4.5.3 Extra Evidence of Amorphicity

As discussed above, the amorphous state is a thermodynamically unstable solid form. It exhibits great molecular mobility and given time will change quite drastically, especially if stored under stressful conditions. The changes which occur center strongly around reverting to a crystalline form. In an attempt to understand this reversion to a crystalline form, a sample of sprayed indomethacin was aged for 5 weeks in a nitrogen environment. The sample was stored at room temperature which stresses the solid by being within 50℃ of its glass transition temperature (Newman 2010). The experimental parameters of the deposition are presented in table 7.

Table 7: Aging Study Experimental Parameters

Experimental Parameters		
Solvent	Acetone	Mw= 58
Solute	IMC	Mw= 358
Flow Rate	0.15	mL/h
Concentration	1.5	%wt
Exposure Time	60	min
Footprint Diameter	3	cm
Working Distance	4	cm
Voltage	7	kV
Date	12/20/2013	

The resulting micrographs of this study are quite striking with respect to the growth and propagation of crystal in an aging amorphous sample. Figure 17 shows an

example of how crystals propagate through an amorphous sample. It also starkly demonstrates the difference in appearance between the sprayed sample (top middle) and crystalline indomethacin (the rest).

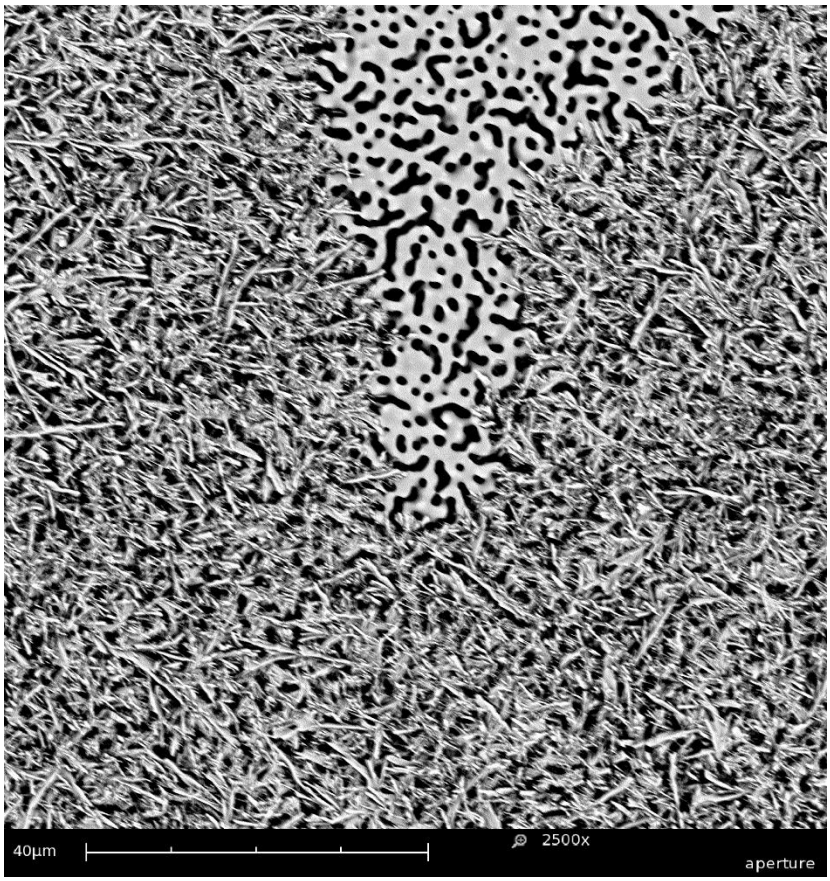

Figure 17: Crystal propagation over aged sample

Figure 18 shows a detail of the boundary between crystal and amorphous indomethacin in the aged sample

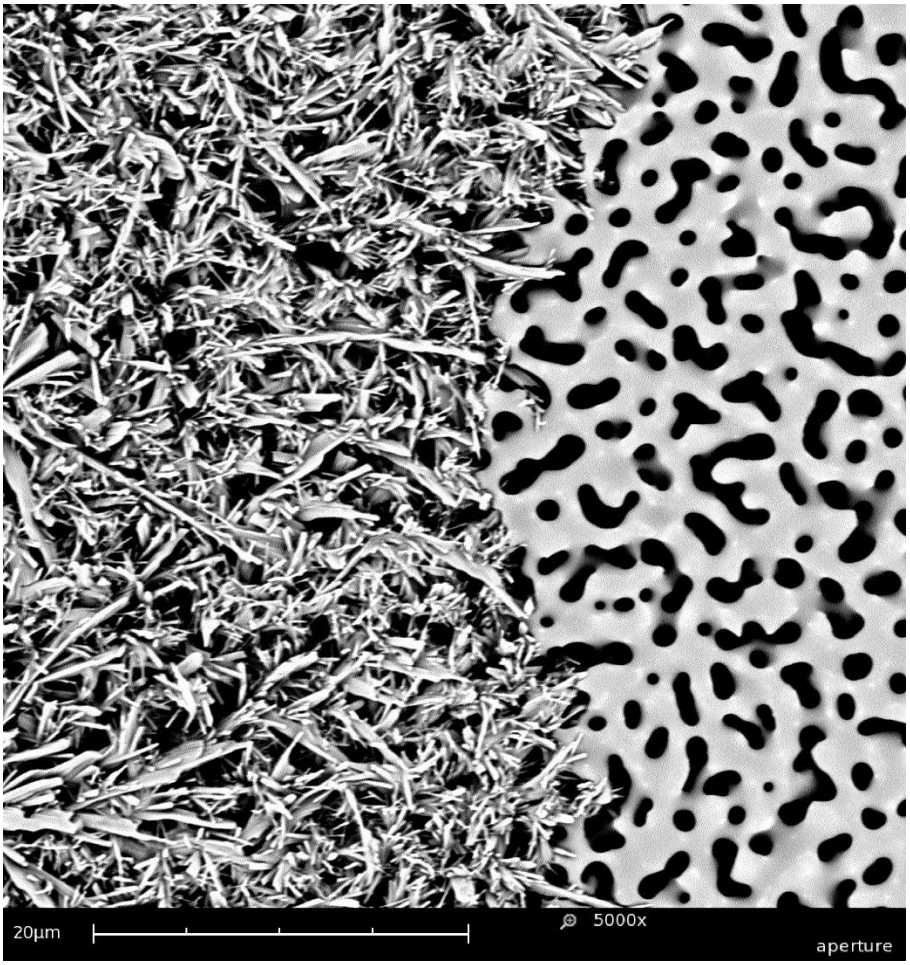

Figure 18: Crystal Propagation detail

The most striking aspect of this micrograph is how amazingly sharp the boundary appears between crystal and amorphous sample. We conclude this is due to a propagation of crystal like a wave through the sample. Initially, crystalline seeds nucleate spontaneously from the amorphous solid and then grow at the boundaries of the amorphous state around it. Figure 19 shows an example of a spontaneously developed crystalline seed.

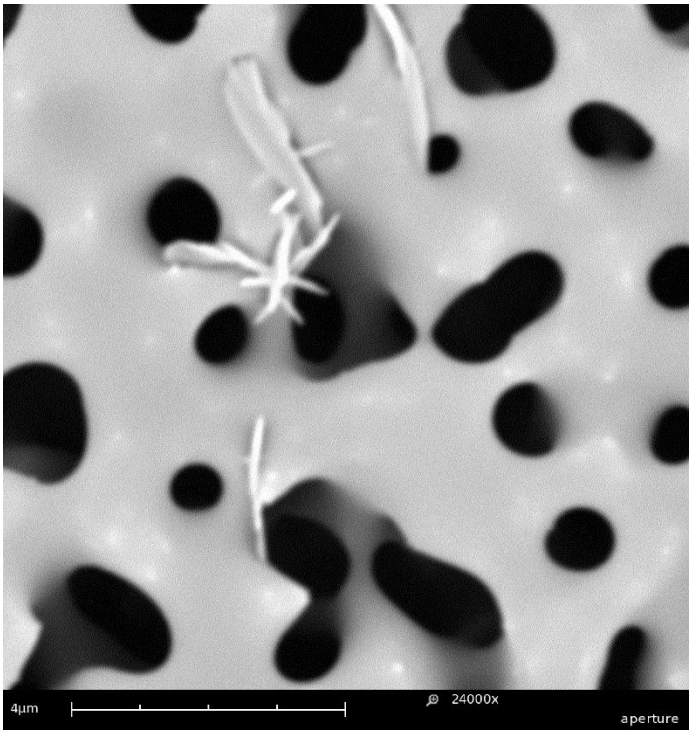

Figure 19: Crystalline seed nucleated from amorphous solid

Because the sample seems to have deteriorated over time to a crystal form, the sample must have started without crystal structure. These aging studies support the diffraction data.

4.6 Solubility Advantage Verification

Solubility data are obtained with UV-Vis spectrophotometry in coordination with Beer's Law. Explorations seek to evaluate the dissolution profile of sprayed indomethacin against crystalline indomethacin. This dissolution profile is then compared to the dissolution profile obtained by Hancock and Parks.

4.6.1 Beers Law

Beer's law expresses the relationship between concentration in solution and absorbance. The explicit statement of Beer's law is stated as

$$A = \epsilon bc. \tag{10}$$

It relates absorbance, defined as

$$A = \log_{10} \frac{P_0}{P}, \tag{11}$$

to the molar absorptivity, optical path length, and concentration of solute.

This simple relationship allows the calculation of concentration of a substance in solution given a fixed path length and known molar absorptivity. Because molar absorptivity depends functionally on wavelength, Beer's law is most appropriately applied at a specific wavelength.

4.6.2 UV Vis Spectrophotometry

A spectrophotometer measures the amount of light a sample absorbs. The device releases a luminous pulse of known intensity through a sample solution and measures the intensity of the light after it leaves the sample. Recalling the definition of absorbance, a decreasing measured intensity clearly accompanies an increasing absorbance.

UV-Vis Spectrophotometry describes a spectrophotometer which operates between the ultraviolet and visual spectra. This type of spectrophotometer is necessary for the analysis of IMC since the 'spectral peaks' of indomethacin occur at 230, 260, and 318 nm which all occur within that range.

4.6.3 Experimental

UV-Vis spectrophotometry, coupled with Beer's law and cuvettes of known optical path length, allows the evaluation of the dissolution profile of spray deposited indomethacin and a crystalline standard. In order to test the dissolution profile, an excess of amorphous sample dissolves into deionized water. Samples are taken periodically as the dissolution proceeds and subjected to spectrophotometry.

In this study, the excess of amorphous sample was determined to be two hours of deposition (roughly three milligrams) in a 50 mL volume of deionized water. Since the saturation solubility of crystalline indomethacin is roughly 1 mg/L, this volume represents a potential 30 fold supersaturation. Since this value could never actualize, it represents an 'excess'. Samples (after the blank sample) were taken every 6 minutes with the first sample being taken 3 minutes after the addition of solute. Similarly, the control study used 3 mg of crystalline IMC (Sigma Aldrich) in 50 mL of de ionized water with samples being taken identically to the amorphous group.

The sample group and control constituted 50 spectral analyses total. The strongest response came from the spectral peak at 260 nm. The value of absorbance at 260 nm was isolated from each spectrum and compiled in a table, paired with its corresponding time. The constant of proportionality (necessitated by Beer's law) was evaluated via the known value of saturation for crystalline indomethacin (.937 mg/L) along with the averaged value of the control sample absorbance. This gave a constant of proportionality as .474 L/mg. After transforming the absorbance data into concentration data, the two data sets

(amorphous and control) were superposed over their identical time scales. The results are presented in Figure 20.

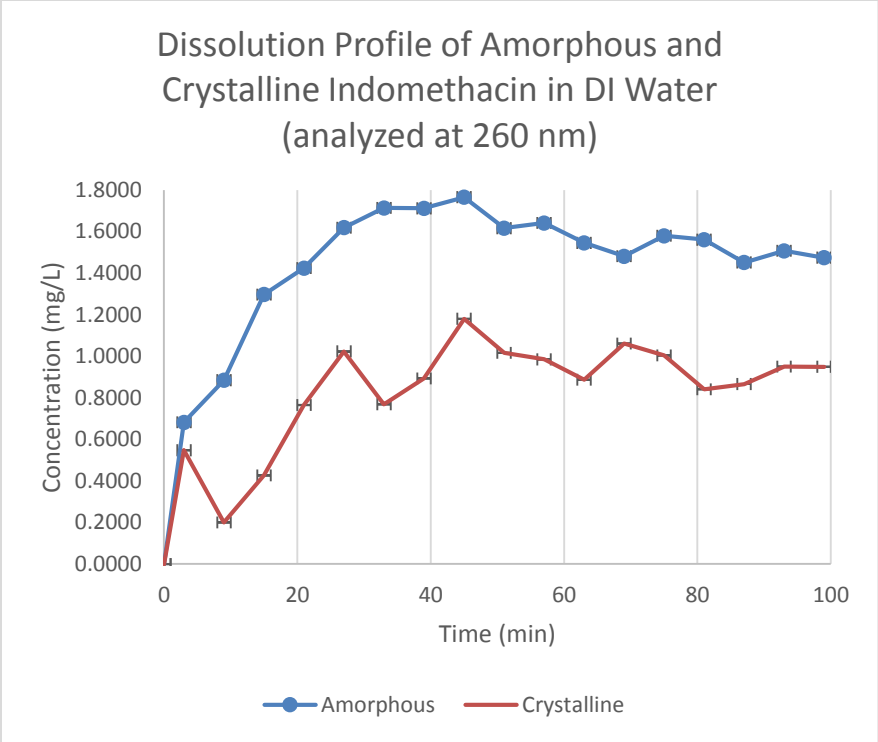

Figure 20: Dissolution Study Results

These results are consistent with data taken from the 318 nm spectral peak, but this profile is omitted due to redundancy. We predict the stark variation and apparent instability in crystalline data derives from sample present concentration gradients and perhaps insufficient mixing. It would seem that the amorphous sample avoided the same problems but the nature of this unpredictable variation in the control is beyond the scope of this investigation. Clearly, the steady state concentration of the amorphous nanoparticles far exceeds that of the crystalline control. In fact, the steady value delivers an 88.5% improvement over the solubility of powdered crystal. It is interesting to note

that the profile of sprayed IMC, though conducted at room temperature, bears a much closer resemblance to the Hancock and Parks amorphous indomethacin dissolution test conducted at 5°C than the test conducted at 25°C. We do not speculate towards reasons or mechanisms for this but observe that the spring is less violent and the parachute substantially more gentle.

CHAPTER 5: CONCLUSIONS

We conclude that electrospray represents an high potential emerging method for the production of amorphous nanoparticles. Electrospray succeeded in producing particles of submicron diameter and aspherical morphology with high monodispersity. These particles evaporated quickly enough to exhibit high amorphicity as well as a substantial aqueous solubility advantage. Coupled with the potential for scale up to industrial throughputs, electrospray presents a strong case for feasible powder production of active pharmaceutical ingredients. Though the particles in this study were deposited on a silicon substrate, the ultimate goal is a powder for pharmaceuticals. This, however, is work which has already been accomplished for other spray drying techniques with cyclone technology.

Other work in post processing involves the solid solution of drug particles with various polymer excipients. The same principles presented in this study apply equally to those efforts. The primary challenge in those explorations is the complexity of the solution. Each case is unique and requires special care. After the solution properties are resolved appropriately, then everything remains practically identical.

REFERENCES

Almeria, B., (2012), "Synthesis of Biodegradable Polymer Micro- and Nanoparticles for Controlled Drug Delivery by Multplexed Electrosprays," Doctoral Dissertation, Yale University.

Amidon, G. L., Lennernas, H., Shah, V. P., and Crison, J. R., (1995), "A Theoretical Basis for a Biopharmaceutic Drug Classification: The Correlation of *in Vitro* Drug Product Dissolution and *in Vivo* Bioavailability," *Pharmaceutical Research*, 12, 413-420.

Andronis, V., Yoshioka, M., and Zografi, G., (1997), "Effects of Sorbed Water on the Crystallization of Indomethacin from the Amorphous State," *Journal of Pharmaceutical Sciences*, 86, 346-351.

Arya, A., Chandra, A., Sharma, V., and Pathak, K., (2010), "Fast Dissolving Oral Films: an Innovative Drug Delivery System and Dosage Form," *International Journal of ChemTech Research*, 2, 576-583.

Babu, N. J., and Nangia, A., (2011), "Solubility Advantage of Amorphous Drugs and Pharmaceutical Cocrystals," *Crystal Growth and Design*, 11, 2662-2679.

Burton, W.K., Cabrera, N. and Frank, F.C. (1951) The growth of crystals and the equilibrium structure of their surfaces. *Philosophical Transactions,* **A243**, 299-358.

Deng, W., Klemic, J. F., Li, X., Reeed, M. A., and Gomez, A. (2006), "Increase of Electrospray Throughput Using Multiplexed Microfabricated Sources for the Scalable Generation of Monodisperse Droplets," *Journal of Aerosol Science*, 37, 696-714.

Deng, W., Waits, C. M., Morgan, B., and Gomez, A. (2009), "Compact Multiplexing of Monodisperse Electrosporays," *Journal of Aerosol Science,* 40, 907-918.

Fahmy, T. M., Samstein, R. M., Harness, C. C., and Saltzman, W. M. (2005b), "Surface Modification of Biodegradable Polyesters with Fatty Acid Conjugates for Improved Drug Targteting," *Biomaterials,* 26, 5727-5736.

Gomez, A., and Tang, K. Q. (1994b), "Charge and Fission of Droplets in Electrostatic Sprays," *Physics of Fluids,* 6, 404-414.

Hancock, B. C., and Parks, M., (2000), "What is the True Solubility Advantage for Amorphous Pharmaceuticals?," *Pharmaceutical Research,* 17, 397-404.

Hancock, B, and Zografi, G, (1997), "Characteristics and Significance of the Amorphous State in Pharmaceutical Systems," *Journal of Pharmaceutical Sciences*, 86, 1-12.

IMS, (2012), "Total Unaudited and Audited Global Pharmaceutical Market by Region," *IMS Health Market Prognosis.*

International Pharmaceutical Excipient Council, (2010), "International Pharmaceutical Excipient Council Glossary", Published by the International Pharmaceutical Excipient Council.

Jain, R. A., (2000), "The Manufacturing Techniques of Various Drug Loaded Biodegradable Poly(Lactide-co-Glycolide) (PLGA) Devices," *Biomaterials,* 21, 2475-2490.

Lojewski, B., Yang, W., Duan, H., Xu, C., and Deng, W. (2013), "Design, Fabrication, and Characterization of Linear Multiplexed Electrospray Atomizers Micro-Machined from Metal and Polymers," *Aerosol Science and Technology,* 47:2, 146-152.

J. W. Mullin, (2001), "Crystallization," *Reed Education and Professional Publishing*

Newman, A., (2010), "Basics of Amorphous and Amorphous Solid Dispersions," in *Seventh Street Development Group*.

Park, J., and Fahmy, T. M. (2010), "Biodegradable Nanoparticles for Drug Delivery," in *Handbook of Nanophysics: Nanomedicine and Nanorobotics,* ed. K. D. Sattler, New York: Taylor and Francis Group, pp. 1-14.

Sarma, B., Chen, J., His, H., and Myerson, A. S., (2011), "Solid forms of Pharmaceuticals: Polymorphs, Salts, and Cocrystals,"*Korean Journal of Chemical Engineering*, 28, 315-322.

Swinney, D. C., and Anthony, J., (2011), "How were new medicines discovered?," *Nature Reviews*, 10, 507-519.

Thayer, A. M., (2010), "Finding Solutions," *Chemical Engineering News*, 88, 13-18.

Volmer, M. and Schultz, W. (1931) Kondensation an Kristalen. *Zeitschrift fur Physikalische Chemie,* **156**, 1-22.

Yamamoto, H., (2012), "Solubilization Technique Based on Solid-Dispersion Techniques with Soluplus® for Poorly Water Soluble Drugs," from *1st Hot-Melt Extrusion Seminar*, Yokohama, Japan.